Astronomy & Astrophysics manuscript no. Steps4_AFhybrids_large_sample_v4
August 27, 2020

Orbital solutions derived from radial velocities and time delays for four *Kepler* systems with A/F-type hybrid pulsations⋆

P. Lampens[1], L. Vermeylen[1], Y. Frémat[1], Á. Sódor[2], M. Skarka[3,4], A. Samadi-Ghadim[5,6], Zs. Bognár[2,7], H. Lehmann[8], P. De Cat[1], A. Goswami[9], and L. Dumortier[1]

[1] Koninklijke Sterrenwacht van België, Ringlaan 3, 1180 Brussel, Belgium
e-mail: patricia.lampens@oma.be
[2] Konkoly Observatory, Research Centre for Astronomy and Earth Sciences, Konkoly Thege M. u. 15-17, H-1121, Budapest, Hungary
[3] Astronomical Institute, Czech Academy of Sciences, Fričova 1, CZ-25165 Ondřejov, Czech Republic
[4] Department of Theoretical Physics and Astrophysics, Masaryk Univerzity, Kotlářská 2, CZ-61137 Brno, Czech Republic
[5] Núcleo de Astronomía, Faculdad de Ingeniería y Ciencias, Universidad Diego Portales, Av. Ejército Libertador 441, Santiago, Chile
[6] Research Institute for Applied Physics and Astrophysics, University of Tabriz, PO Box 51664, Tabriz, Iran
[7] Eötvös Loránd University, Institute of Physics, Pázmány Péter sétány 1/A, H-1171, Budapest, Hungary
[8] Thüringer Landessternwarte, Tautenburg, Germany
[9] Indian Institute of Astrophysics, II Block, Koramangala, Bangalore 560 034, India

Received...; accepted ...

ABSTRACT

Context. The presence of A/F-type *Kepler* hybrid stars extending across the entire δ Sct-γ Dor instability strips and beyond remains largely unexplained. In order to better understand these particular stars, we performed a multi-epoch spectroscopic study of a sample of 49 candidate A/F-type hybrid stars and one cool(er) hybrid object detected by the *Kepler* mission. We determined a lower limit for the multiplicity fraction of 27%. For six spectroscopic systems, we also reported long-term variations of the time delays. For four of them, the time delay variations are fully coherent with those of the radial velocities (RVs) and can be attributed to orbital motion.
Aims. We aim to improve the orbital solutions for those spectroscopic systems with long orbital periods (order of 4-6 years) among the *Kepler* hybrid stars that we continued to observe.
Methods. The orbits are computed based on a simultaneous modelling of the RVs obtained with high-resolution spectrographs and the photometric time delays (TDs) derived from time-dependent frequency analyses of the *Kepler* light curves.
Results. We refined the orbital solutions of four spectroscopic systems with A/F-type *Kepler* hybrid component stars: KIC 4480321, 5219533, 8975515 and KIC 9775454. Simultaneous modelling of both data types analysed together enabled us to improve the orbital solutions (all systems), obtain more robust and accurate information on the mass ratio (some for the first time), and identify the component with short-period δ Sct-type pulsations (all systems). The information gained is maximized when one of the components, generally the one exhibiting the δ Sct-type pulsations, is the fast(er) spinning component. In several cases, we were also able to derive new constraints for the minimum component masses.

1. Introduction

In an effort to understand and unravel the enigma of the low frequencies in the brighter A/F-type candidate hybrid pulsators of the *Kepler* mission (Grigahcène et al. 2010; Balona et al. 2015), we started a radial-velocity monitoring campaign with high-resolution échelle spectrographs located in various European observatories. Our goal is to characterize the spectroscopic variability of an unbiased sample of *Kepler* hybrid (γ Dor - δ Sct) pulsators. This programme was initiated during the middle of 2013. We collected multi-epoch observations (4 - 6 times at least) in order to detect binarity or multiplicity at the different time scales, with orbital periods ranging from a few days to several years, and to establish a meaningful classification. We determined the epoch radial velocities, projected rotational velocities, new or improved atmospheric stellar properties (i.e. $T_{\rm eff}$, $\log g$, $v \sin i$), and we provided a classification in terms of multiplicity, pulsation and/or (fast) rotation for all our targets on the basis of the shapes of the cross-correlation functions and their radial velocities as a function of time.

In our first study, we followed a sample of 49 candidate hybrid stars and one much cooler hybrid object identified by Uytterhoeven et al. (2011). We found a significant rate of short- and long-period binary as well as multiple systems as we detected 10 spectroscopic systems in total, i.e. 4 double-lined (SB2) systems, 3 triple-lined (SB3) systems, 4 single-lined (SB1) systems (only 3 belong to the A/F-class), and 3 objects with long-term radial-velocity variations (VAR). We determined the orbital solutions of seven systems. For two hierarchical triple systems, we also proposed a preliminary solution for the outer orbit. Using the classification results, we provided a lower limit of the fraction of A/F-type hybrid pulsators which belong to spectroscopic binary and multiple systems. Including the known *Kepler* eclipsing binary we derived a multiplicity fraction of (at least) 27%. Two other hybrid targets have a possible companion or shell (CMP). If we count these two targets, we obtain an overall multiplicity fraction of about 30% among these candi-

⋆ This study is based on spectra obtained with the HERMES échelle spectrograph installed at the Mercator telescope, operated by the IvS, KULeuven, funded by the Flemish Community and located at the Observatorio del Roque de los Muchachos, La Palma, Spain of the Instituto de Astrofísica de Canarias.

Table 1: List of targets and general properties of the RV data.

KIC ID	Nr	BJD start 2,450,000.+	BJD end 2,450,000.+	Time range (from/to)	Instr.[2]
4480321	61	5820.4499	8676.4431	15/09/2011 - 11/07/2019	H1
5219533	52	5372.7083	8792.3578	25/06/2010 - 04/11/2019	H1
8975515	31	5345.7088	8792.3686	29/05/2010 - 04/11/2019	H1
9775454	26	5345.7325	8794.3056	29/05/2010 - 06/11/2019	H1
9775454	2	8231.4431	8232.3771	22/04/2018 - 23/04/2018	H2

Notes. [(2)] H1 stands for 'HERMES'. H2 stands for 'HESP'.

date hybrid pulsators (Lampens et al. 2018, from hereon Paper I).

Among the new spectroscopic systems, we identified several cases for which analysis of the *Kepler* time delays (TDs) (mostly derived from the short-period pulsation frequencies) with the radial velocities (RVs) enables us to derive improved orbital elements, accurate mass ratios as well as a (most) probable identification of the pulsating component. The goal of this paper is to determine orbital solutions for these systems as accurately as possible based on the results of a unified modelling by combining the various data types into a single, simultaneous analysis. In the present study, we will make usage of the radial velocities acquired with the échelle spectrograph HERMES equipping the 1.2-m Mercator telescope, La Palma, Spain (Raskin et al. 2011) available from Paper I (see table C.2). Furthermore, we reported variable TDs in nine cases, in particular for the spectroscopic systems KIC 4480321, 5219533, 8975515, and KIC 9775454 (Paper I, fig. 24). For all four systems, our spectroscopic observations were acquired until late 2019. For KIC 9775454, we included the measurements obtained in 2018 with the high-resolution échelle spectrograph HESP (R = 60,000) mounted at the Himalayan Chandrasekhar telescope (HCT), operated by the IIA, Bangalore, India[1]. Consequently, all RV data of all four systems and their components were updated to the latest possible date. First, we present the current status of each individual system (Sect. 2). In Sect. 3, we introduce the methodology for computing the refined orbits. Sect. 4 provides the orbital solutions using simultaneous modelling. In Sect. 5, we present and discuss the distributions of the frequency spacings in the high-frequency region of the Fourier transforms of each system. Finally, we present our conclusions for all the treated systems (Sect. 6).

2. Presentation of the systems

We present a summary of useful high-resolution spectra for each of the four systems listed in Table 1. In addition to the total number of spectra available for each system, we also mention the spectrograph and the time basis. The revised orbital solutions (Sect. 4) are thus based on the combination of updated sets of component RVs and the time delays (TDs) previously derived from time-dependent frequency analyses of the oscillations detected in the *Kepler* light curves (Paper I), providing us with a total time basis longer than eight years for each case.

[1] https://www.iiap.res.in/hesp

2.1. KIC 4480321

KIC 4480321 (HD 225479, V=10.3, A9 Vwkmet) is a hybrid variable star revealed by Uytterhoeven et al. (2011), with frequencies in the ranges [0.2, 5.0] d^{-1} and [5.1, 61.2] d^{-1} and a most dominant frequency of 0.710 d^{-1} in the γ Dor region. The star was also reported as rotationally variable (Nielsen et al. 2013), with g-mode multiplets split by rotation. The period spacings in the γ Dor region were obtained by Li et al. (2019). This star was classified as a SB3 from our multi-epoch study. It is an hierarchical system, with a twin-like inner binary consisting of early F-type stars orbiting a slightly more luminous and more rapidly rotating A-type companion (we used the basic model of an A5-star, $v \sin i$ = 160 km s^{-1} with 2 F0-stars, $v \sin i$ = 10 km s^{-1}, Paper I). We derived an orbital solution for the inner pair with a 9.1659 d period, and an outer orbital solution with an estimated 2280 d period, and reported the existence of variable TDs in excellent agreement with the proposed solution for the outer orbit. We determined the component effective temperatures $T_{\rm eff\ 1}$ = 7900 ± 100 K and $T_{\rm eff\ 2}$ and $T_{\rm eff\ 3}$ ranging between 6300 and 6900 K (the latter components have almost similar temperatures), assuming $\log g$ = 4 (Paper I, Sect. 6.3). Murphy et al. (2018, Annex C3) reported P = 2270 ± 60 d for the outer orbit from a modelling of Lampens et al. (2018)'s RV measurements in combination with their time delays.

2.2. KIC 5219533

KIC 5219533 (HD 226766, BU 1474 B, V=9.2, A2-A8, Renson & Manfroid (2009)) is the visual companion of BU 1474 A at an angular separation of 65" (HD 189178, V=5.44, B5 He weak, Renson & Manfroid (2009); also a spectroscopic binary). This star was classified as a *Kepler* hybrid variable star by Uytterhoeven et al. (2011), with frequencies in the ranges [0.3, 4.6] d^{-1} and [5.4, 29.9] d^{-1}, and a dominant frequency of 10.285 d^{-1} Uytterhoeven et al. (2011, Table 3). It was recognized as a new SB3 based on the multi-epoch spectra. The system is hierarchical, consisting of an inner pair with two nearly identical stars of spectral type near A5 and a more rapidly rotating outer component of a slightly cooler type. For both components of the inner pair, the mean effective temperatures of $T_{\rm eff\ 1}$ = 8300 ± 100 K and $T_{\rm eff\ 2}$ = 8200 ± 100 K and projected rotational velocities of 10 km s^{-1} were obtained coupled to the light factor l_1 = 0.53 ± 0.02, assuming $\log g$ = 4 (Paper I, Sect. 6.4). Component C has $v \sin i$ equal to 115 km/s Uytterhoeven et al. (2011). An orbital solution with P_{orb} = 31.9181 d was derived for the inner pair, while a tentative outer orbit was proposed with $P_{orb} \sim$ 1600 d. Later on, Murphy et al. (2018, Annex C4) studied this system using the phase modulation (PM) method (Murphy et al. 2014). They derived a very high mass function and proposed that the third body is a δ Sct star with an orbital period longer than 1500 d. Simultaneously with Lampens et al. (2018), Catanzaro et al. (2019b,a) independently observed the system (from 2014 to 2018) with the aim to characterize the orbits, and to perform a chemical analysis of its components. They proposed the orbital parameters based on their and Lampens et al. (2018)'s RVs (P_1 = 31.9187 d, e_1 = 0.28, q_1 = 1.03 and P_2 = 1615 d, e_2 = 0.54, $f(M_{1,2})$ = 0.18) which confirm the findings of Paper I. They also derived the atmospheric properties $T_{\rm eff}$, $\log g$, and $v \sin i$ based on 2 spectra (obtained at max RV separation) and chemical abundances based on one spectrum (max S/N), first for two components, next with the third one included. However, they were unable to derive the chemical composition of component

C (except for Mg II). They concluded that both components of the close pair are twin Am stars (with underabundances of C, O, Mg, Ca and Sc and overabundances of Na, Fe-peak elements). From the simple assumption that all the components have equal mass, they suggested that the orbits might be coplanar. All previous studies explicitly mention that more data for this multiple system are needed.

2.3. KIC 8975515

KIC 8975515 (HD 188538, V=9.5, A6 V:) was classified as a *Kepler* hybrid star by Uytterhoeven et al. (2011). The star shows frequencies in the ranges [0.3 - 4.7] d^{-1} and [5.3 - 25.8] d^{-1} of the γ Dor and the δ Sct pulsation regimes respectively, with the dominant frequency of 13.97 d^{-1} (Uytterhoeven et al. 2011, Table 3). Therefore, we included it among our sample of A/F-type candidate hybrid stars to be monitored spectroscopically where it was recognized as a new SB2 from the multi-epoch observations. The system consists of two A-type stars of similar temperature but with dissimilar projected rotational velocities, forming an eccentric system (e = 0.409 ± 0.015). From a detailed spectrum fitting using the code SYNSPEC (Hubeny & Lanz 1995) and the ATLAS-9 atmosphere models (Castelli & Kurucz 2003) in order to build a suitable composite model in the spectral range [500-520] nm, the mean effective temperatures $T_{\rm eff\ 1}$ = 7440 ± 20 K and $T_{\rm eff\ 2}$ = 7380 ± 21 K with the light factor l_1 of 0.65 ± 0.03 (component A), assuming $\log g = 4$, were obtained. The mean projected rotation velocities were consistently determined as 162 ± 2 and 32 ± 1 km s^{-1} (Paper I, Sect. 6.12). Lampens et al. (2018) proposed a preliminary orbit with a period of the order of 1600 d, in line with the TD curve, while Murphy et al. (2018, Annex C12) obtained a solution with a shorter period of 1090 d, using the published RVs in combination with their time delays (TDs). They furthermore assumed that the narrow-lined component is the δ Scuti pulsator and reported a slight aperiodicity in their derived TDs.
An extensive study of its pulsational properties was recently published by Samadi-Ghadim et al. (2020). They concluded that both components are pulsating, the fast-rotating component is a pulsating hybrid star also showing retrograde r modes, while the more slowly-rotating component is a δ Scuti pulsator.

2.4. KIC 9775454

KIC 9775454 (HD 185115, V=8.2, F1 Vs) is a candidate hybrid variable star from Uytterhoeven et al. (2011), with frequencies in the ranges [0.2, 4.6] d^{-1} and [14.7, 14.9] d^{-1} and a dominant frequency of 4.161 d^{-1}. It has a Gaia DR2 RV of -20.22 ± 1.02 km/s (Gaia Collaboration 2018). The atmospheric parameters derived from high-resolution spectroscopy are $T_{\rm eff}$ = 7287 K and $\log g$ = 4.25 with a projected rotation velocity of $v \sin i$ = 65 km s^{-1} (Paper I, Table C.1). Lampens et al. (2018) classified this object as a long-term SB1 of unknown orbital period. The CCF of the composite spectrum shows a broad-lined component blended with a narrow-lined component. Murphy et al. (2018, Annex C14) proposed an orbit with P_{orb} = 1686 ± 13 d and e = 0.23 ± 0.02 by combining the published RVs with their TDs. In this case, the secondary component contributes only weakly to the composite spectrum. Nevertheless, we were able to obtain some individual RVs for this much cooler component (cf. Sect. 4.4).

3. Methodology

The orbital motion of a binary system causes a periodic fluctuation of the light path and its associated travel time with respect to the system's centre of mass. On the other hand, light from a source in motion undergoes a (Doppler) shift of its frequency. In the frequency domain (for a time base T » P_{orb}), this phenomenon corresponds to a frequency modulation (FM) which can be detected as a frequency multiplet whose exact spacing is the orbital frequency (Shibahashi & Kurtz 2012). In the time domain (for T « P_{orb}), this effect corresponds to a modulation of the phase (PM) with the orbital period, whose amplitude depends on the mass of the (unseen) companion and the observed frequency (Murphy et al. 2014). Hence, if one of the components is a pulsating star, the change in the light travel time introduces periodic phase shifts of each individual (pulsation) frequency. By converting the phase shift into a time delay, the frequency dependency is removed. Therefore, if the star is a multiperiodic pulsator, all the pulsation frequencies will experience the same time delay.
Murphy et al. (2014) described the principle of obtaining time delays from observed phase shifts of the pulsations and applied the PM method unto various cases of *Kepler* pulsating stars in (non-eclipsing) binary systems, while Murphy & Shibahashi (2015) provided an analytical method for solving the orbit, also in highly eccentric cases. This method is in essence similar to the search for variability in the (O-C)'s, the residuals in the times of specific phases in the light curve of periodically pulsating stars which are members of a binary system, e.g. BL Cam (Fauvaud et al. 2006, 2010). Murphy et al. (2016) presented examples of orbital analyses combining radial velocities (RVs) with photometric time delays (TDs), and discussed some of the limitations and advantages. In this study, we developed and applied our own code for a simultaneous least-squares fitting of our updated RVs and the TDs based on the *Kepler* data. Both quantities are functions of the same orbital parameters: the time delay corresponds to the light travel time and the radial velocity is the time derivative of the position along the orbital path projected in the observer's direction. We consider the following equations as our model:

$$TD(t) = \frac{asini}{c}\frac{1-e^2}{1+ecos(\nu(t))}(sin(\nu(t)+\omega) + l + mt \quad (1)$$

$$V(t) = 2\pi\frac{asini}{P\sqrt{1-e^2}}(cos(\nu(t)+\omega) + ecos\omega) + V_\gamma \quad (2)$$

where the mean motion ν is a function of t, T_0, P and e, T_0 is the time of periastron passage, P is the orbital period, $a \sin i$ is the projected semi-major axis, e is the eccentricity, ω is the longitude of the periastron, l is a constant, m is the slope of the linear trend, and V_γ is the systemic velocity. Equation 1 is given by Irwin (1952) (see Pribulla et al. 2005). We remark that Equ. 1 allows to correct the original TDs by including a linear trend. This correction is necessary to convert the pulsation frequencies to their mean values corresponding to the motion of the centre-of-mass of the system, since the frequencies used for constructing the TDs may be biased by the uneven orbital phase coverage of the *Kepler* data, and such a bias will introduce a linear trend in the TDs themselves (cf. the (O-C) curves).

In Paper I, we computed the time-dependent phases for up to 20 frequencies of highest S/N (generally the ones located in the p-mode regime) for all 49 targets of our sample. We thus uncovered nine objects for which correlated variations of comparable amplitude in the TDs were observed. In six systems, we could attribute the TD variations to orbital motion of a binary or multiple system. By analysing the RV and the TD data together, we are able to refine the orbital solutions and obtain stronger constraints on (some of) the orbital parameters and their derived parameters. Since the TDs are generally determined from the high(er) frequencies, they only provide information on the origin of the δ Scuti-type pulsations associated to these frequencies. However, the low(er) frequencies (γ Doradus-type) may still originate from any component. In the next sections, we will analyse each of the four systems just described and highlight the gains that may be obtained from such modelling.

4. Orbital solutions from combined modelling

4.1. The triple system KIC 4480321

KIC 4480321 is a triple system (SB3) whose orbital periods are estimated to be 9.166 and ~ 2280 d (Sect. 2.1). We computed the phase shifts and their associated TDs for frequencies of highest S/N and evidenced the presence of long-term variations which are coherent with the long-term RV variability (Paper I, fig. 24). We remark that the TDs were corrected by removing a linear trend from the original data (as everywhere). We then performed a simultaneous least-squares fitting of three updated component RVs and the mean TDs with their respective uncertainties. The best fit in the sense of min. χ^2 was obtained when we associated the TDs with the RVs of the fast spinning, more luminous A-type star (component C). Fig. 1 illustrates the quality of the fit showing the outer orbital solution together with both data types. The TDs and the RVs are overlaid with the AB-C orbital solution. Note that the TD curve mimics the RV curve but with an apparently larger eccentricity and a 90°shift in periastron longitude (Irwin 1952). The revised orbital parameters of the coupled solutions are listed in Table 2. Compared to Paper I, we see that the orbital solution of the A-B system is robust and well-determined while the outer orbital solution changed profoundly. The orbital period is longer (P ~ 2380 days) and better determined than before (see also Murphy et al. 2018), while the eccentricity and the semi-axis major increased substantially. Thus, the minimum component mass $M_{\rm C} \sin^3 i_{out}$ increased to 1.60 ± 0.05 $M_\odot$. The strongest improvement concerns the accuracy and robustness of the outer orbital solution. This is due to two things: (a) by combining both data types, we dispose of a time base longer than eight years and (b) the TDs concern the fast-rotating component C for which the RVs show the largest scatter. We therefore were able to determine a (much) improved mass ratio for the outer system and to provide (more) reliable values of the three minimum component masses. From the minimum total mass of the A-B system derived for each orbit, we get $\sin i = \left((M_{\rm A}+M_{\rm B})\sin^3 i\right)^{1/3}\left(M_{\rm AB}\sin^3 i_{out}\right)^{-1/3}\sin i_{out}$, from which we obtain the condition $i < 58°$for the inner orbit. We may furthermore attribute the δ Scuti pulsations to the more massive component C (the frequencies showing phase shifts are all located in the p-mode region). In summary, KIC 4480321 is a hierarchical triple system with $q_{in} = \frac{M_B}{M_A} = 0.98$ and $q_{out} = \frac{M_C}{M_{AB}} = 0.68$.

Table 2: Values and standard deviations of the constrained orbital parameters for KIC 4480321. Note that from hereon, for all similar tables, T_0 is expressed in Hel. JD - 2,400,000.

Orbital solution A-B		
Orbital parameter	Value	Std. dev.
P (d)	9.16585	0.00015
T_0 (Hel. JD)	58503.065	0.015
e	0.07894	0.00097
ω (°)	351.1	0.6
V_0 (km s^{-1})	(var.)	
$a_{\rm A}\sin i$ (AU)	0.04779	0.00006
$a_{\rm B}\sin i$ (AU)	0.04876	0.00006
$K_{\rm A}$ (km s^{-1})	56.90	0.07
$K_{\rm B}$ (km s^{-1})	58.05	0.07
$M_{\rm A}\sin^3 i$ ($M_\odot$)	0.7216	0.0019
$M_{\rm B}\sin^3 i$ ($M_\odot$)	0.7073	0.0019
$q_{\rm in}$	0.980	0.002
$rms_{\rm A}$ (km s^{-1})	1.486	
$rms_{\rm B}$ (km s^{-1})	0.455	
Orbital solution AB-C		
Orbital parameter	Value	Std. dev.
P (d)	2381.	5.9
T_0 (Hel. JD)	59082.	13.
e	0.140	0.006
ω (°)	197.9	1.8
V_0 (km s^{-1})	-19.97	0.04
$a_{\rm AB}\sin i_{out}$ (AU)	2.232	0.013
$a_{\rm C}\sin i_{out}$ (AU)	3.293	0.076
$a_{\rm TD_C}$ (d)	0.0190	0.0004
$K_{\rm AB}$ (km s^{-1})	10.30	0.07
$K_{\rm C}$ (km s^{-1})	15.20	0.35
$M_{\rm AB}\sin^3 i_{out}$ ($M_\odot$)	2.36	0.12
$M_{\rm C}\sin^3 i_{out}$ ($M_\odot$)	1.60	0.05
$q_{\rm out}$	0.678	0.016
$rms_{\rm C}$ (km s^{-1})	4.689	
$rms_{\rm TD}$ (d)	0.0012	

4.2. The triple system KIC 5219533

KIC 5219533 was classified as triple (SB3) with an inner pair of Am-like stars and with orbital periods of 31.919 and ~ 1615 d (Sect. 2.2). For this system, we also detected long-term variations of the TDs in agreement with the long-term change observed in the RVs (Paper I, fig. 24). We performed a simultaneous least-squares fitting of the updated component RVs and the mean TDs with their respective uncertainties, and obtained the best fit in the sense of min χ^2 with the TDs assigned to the outer companion (component C). Since this component is heavily diluted in the composite spectrum, its RVs are not well-determined. However, a modelling of the combined data allows to derive full orbital solutions. The new parameters of the inner and outer orbital solutions are presented in Table 3. Fig. 2 illustrates the quality of the fit as well as both solutions. The mean residuals of the component RVs stay below 1 km s^{-1}. The orbital solution of the A-B pair is in good agreement with the one proposed by Catanzaro et al. (2019b), though our semi-major axes are slightly larger (and our component masses a bit smaller) than theirs. Indeed, their Figs. 3 and 4 show that several HERMES RVs (open symbols) lie a bit off from their final solution. The overall gain in accuracy for most parameters of the inner orbital solution is a factor of 5, while the orbital

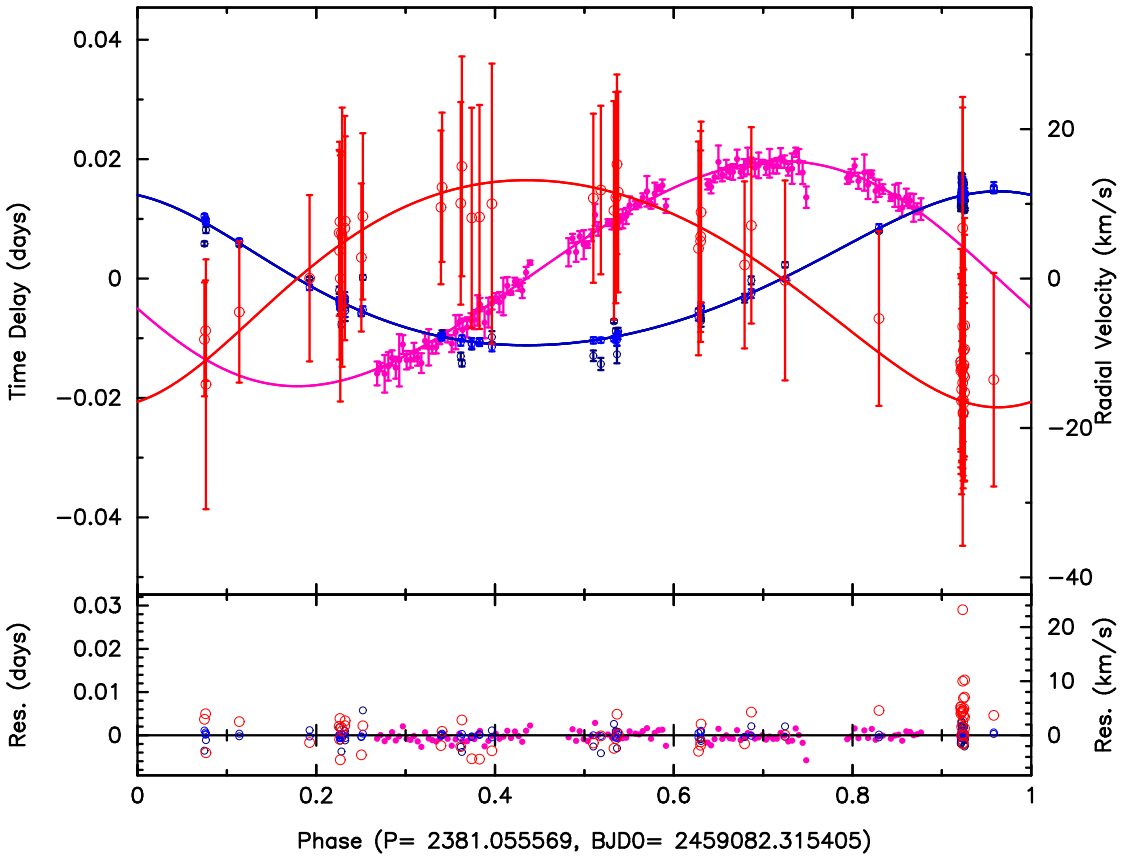

Fig. 1: Data and outer orbital solution for KIC 4480321. The time delays and radial velocities (resp. filled pink and unfilled red symbols for component C; blue symbols for the centre of mass of components A and B) are overlaid with the AB-C orbital solution (solid lines). The residuals are shown in the bottom panel.

period is 10 times more accurate. We cannot compare the mean RV residuals since these were not displayed. In Fig. 2 (right), the TDs and the RVs are plotted together with the revised AB-C orbital solution. We thus determined the semi-axis major of component C and the minimum mass of the A-B pair for the first time. The gain is largest for the outer orbit since the accuracy on the parameters improved with a mean factor of 10 while the orbital period is about 30 times more accurate compared to Catanzaro et al. (2019b). In particular, we obtained the minimum component masses $M_{\rm A}\ \sin^3 i = 1.336 \pm 0.005$, $M_{\rm B}\ \sin^3 i = 1.293 \pm 0.004$ and $M_{\rm C}\ \sin^3 i_{out} = 1.47 \pm 0.02$ M$_\odot$. From the minimum total mass of the A-B system derived for each orbit leading to the condition $\sin i_{out} = 0.996\ (\pm\ 0.009)\ \sin i$, we infer that both orbits are very close to coplanarity. In summary, KIC 5219533 is a hierarchical, probably coplanar system with $q_{in} = 0.97$ and $q_{out} = 0.57$. We furthermore established that the δ Scuti pulsations are linked is the more massive, faster rotating star in the system.

4.3. KIC 8975515

This star was recognized as SB2 from our multi-epoch study, and also shows long-term variations of the TDs coherent with the variations found in the RVs (Paper I, fig. 24). The system consists of late A-type stars with one fast spinning (component A) and one (apparently) slowly spinning star (component B). In Paper I, we derived an orbital solution of type SB1 based on the RVs of component B only ($P_{orb} \sim 1600$ d). We first derived a pure RV-based orbital solution (using the RVs of both components). Unfortunately, the extreme uncertainties on the RVs of the fast spinning component didn't allow to constrain its RV amplitude. This is obvious in Fig. 3 (left) which illustrates the best-fit orbital solution with a period of 1581 d. Subsequently, we performed two simultaneous (RV+TD) analyses, by associating the TDs with each set of RVs in turn, and found an optimum fit when the TDs were assigned to component A.

We determined an orbital period of 1603.4 ± 9.3 d. The new orbital parameters and their derived fundamental properties are listed in Table 4. The residuals show the very good agreement between both data types, with small mean residuals for the TDs and RVs of component B (the slower rotator), and a large (non-zero) mean residual for component A (the faster rotator). The orbital solution is illustrated in Fig. 3 (right). In this case, the mass ratio (q = 0.83 ± 0.05) is well-determined thanks to the high accuracy of the TDs (whereas the corresponding component RVs show a very large scatter). The present method allowed us to derive information which was otherwise impossible to obtain with a pure RV-based solution. Another conclusion is that the faster rotating component exhibits the δ Scuti pulsations. This may also explain why the RV residuals of component A are found to be systematically off from the final solution. From the parameters displayed in Table 4, we obtain the minimum masses, $M_{\rm A}\ \sin^3 i = 0.0195 \pm 0.0024$ and $M_{\rm B}\ \sin^3 i = 0.0161 \pm 0.0011$ M$_\odot$. Assuming that either one of the components has a typical mass of ~ 2 M$_\odot$, we expect that the system is seen under a low inclination angle (approx. 12°).

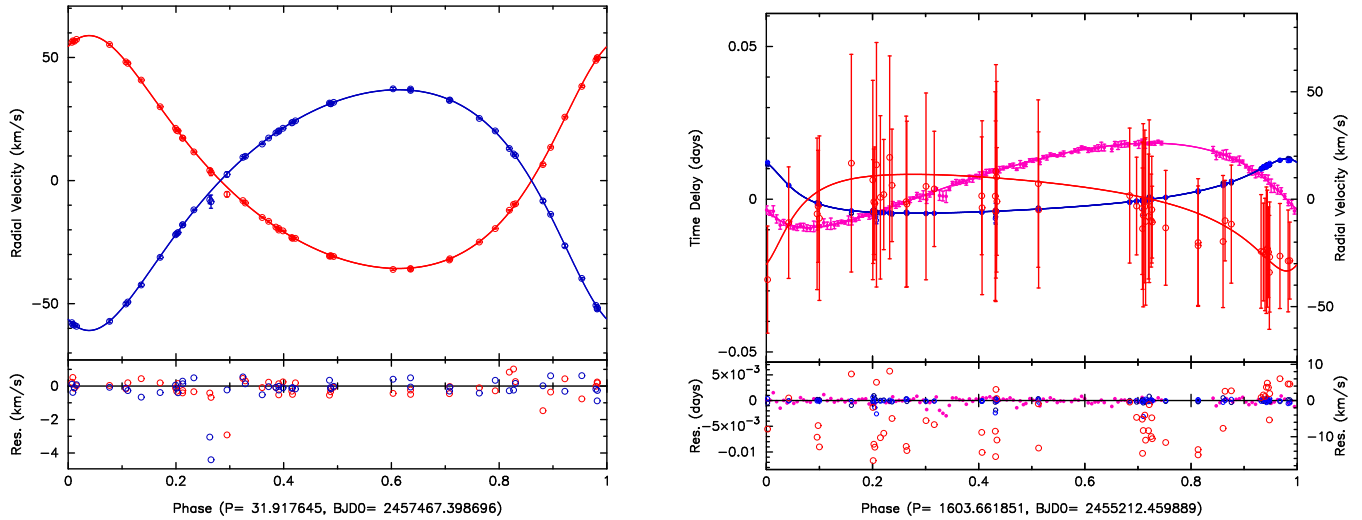

Fig. 2: Data and orbital solutions for KIC 5219533. *Left:* Inner orbit based on the HERMES RVs. The radial velocities (red symbols for component A; blue symbols for component B) are overlaid with the A-B orbital solution (solid lines). The largest residuals are found near the nodal passage. *Right:* Outer orbit based on the HERMES RVs and the TDS from the *Kepler* photometry. The time delays and radial velocities (resp. filled pink and unfilled red symbols for component C; blue symbols for the centre of mass of components A and B) are overlaid with the AB-C orbital solution (solid lines). The residuals are shown in the bottom panels.

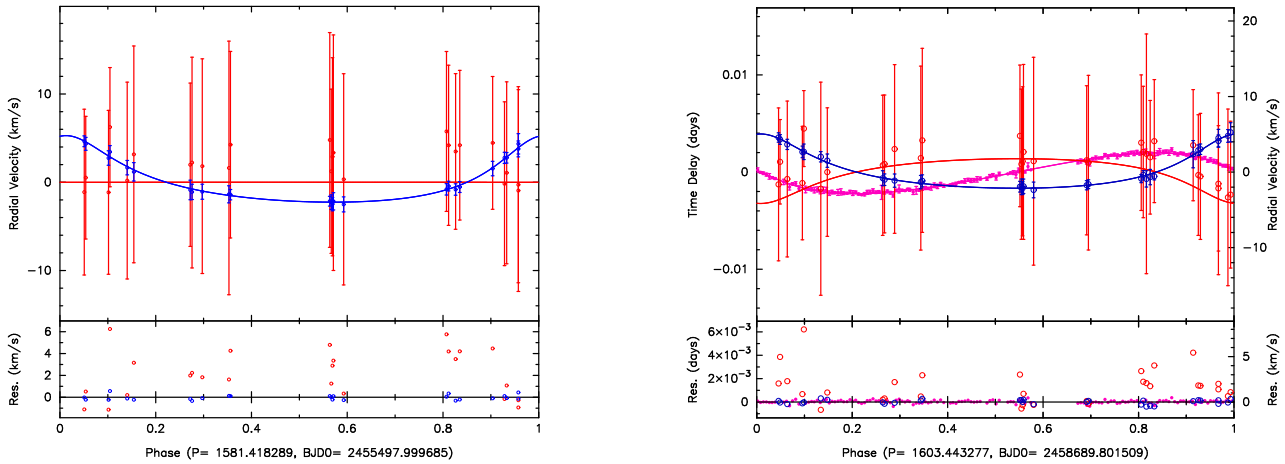

Fig. 3: Data and orbital solution (KIC 8975515). *Left:* Orbit (nr 1) based on the HERMES RVs. The RVs (red symbols for component A; blue symbols for component B) are overlaid with a preliminary orbital solution of type SB2, however without any constraint on the amplitude K_A. *Right:* Orbit (nr 2) based on the HERMES RVs and the TDs from the *Kepler* photometry. The time delays and radial velocities (resp. filled pink and unfilled red symbols for component A; blue symbols for component B) are overlaid with the A-B orbital solution (solid lines). The residuals are shown in the bottom panels.

4.4. KIC 9775454

KIC 9775454 was classified as a long-period SB1 (Sect. 2.4). It was shown to display long-term variations of the TDs in agreement with the orbital variations of the RVs (this concerns also the dominant frequency located at 4.161 d^{-1}, cf. Paper I). Murphy et al. (2018) used the HERMES RVs of the broad-lined primary (component A) and derived an orbital solution with a period of ∼1700 days from their combined (RV+TD) analysis. Being much fainter, component B was not directly detected in the high-resolution spectra. Nevertheless, we managed to obtain RV measurements which indicated the presence of a cool secondary by using a mask of type K0 and computing cross-correlation functions (CCFs) of the residual spectra (after proper subtraction of an adequate synthetic spectrum to remove the contribution of the primary). The CCFs were computed for the spectral range [5100 - 5700] Å. These "residual" CCFs revealed a small peak whose Doppler shifts appear to behave in anti-correlation with those of component A (see Fig. 5). In this way, we were able to extract additional RV data. We roughly estimated their uncertainties from the widths of the associated spectral lines. Thus, we can classify KIC 9775454 as a SB2. We next performed a simultaneous (RV+TD) analysis, by fitting the component RVs together with the TDs assigned to the broad-lined primary (component A). The new orbital solution is illustrated by Fig. 4. The RV residuals of component A and the TD residuals are within expectation while the RV residuals of component B are systematically large. This can be explained by the noisy "residual" CCFs associated to the difficulty of identifying the lines of the cool component in the spectra. The orbital parameters and derived fundamental properties are listed in Table 5. These parameters agree very

Table 3: Values and standard deviations of the constrained orbital parameters for KIC 5219533.

Orbital solution A-B		
Orbital parameter	Value	Std. dev.
P (d)	31.91763	0.00022
T_0 (Hel. JD)	57467.41	0.02
e	0.271	0.001
ω (°)	335.3	0.2
V_0 (km s^{-1})	(var.)	
$a_{\rm A}\sin i$ (AU)	0.13369	0.00019
$a_{\rm B}\sin i$ (AU)	0.13810	0.00023
$K_{\rm A}$ (km s^{-1})	47.33	0.07
$K_{\rm B}$ (km s^{-1})	48.90	0.08
$M_{\rm A}\sin^3 i$ (M$_\odot$)	1.336	0.005
$M_{\rm B}\sin^3 i$ (M$_\odot$)	1.293	0.004
$q_{\rm in}$	0.968	0.002
$rms_{\rm A}$ (km s^{-1})	0.550	
$rms_{\rm B}$ (km s^{-1})	0.833	
Orbital solution AB-C		
Orbital parameter	Value	Std. dev.
P (d)	1603.5	1.7
T_0 (Hel. JD)	55212.9	3.2
e	0.564	0.004
ω (°)	210.6	0.5
V_0 (km s^{-1})	10.70	0.04
$a_{\rm AB}\sin i_{out}$ (AU)	1.542	0.008
$a_{\rm C}\sin i_{out}$ (AU)	2.74	0.03
$a_{\rm TD_C}$ (d)	0.0158	0.0002
$K_{\rm AB}$ (km s^{-1})	12.67	0.08
$K_{\rm C}$ (km s^{-1})	22.49	0.27
$M_{\rm AB}\sin^3 i_{out}$ (M$_\odot$)	2.60	0.07
$M_{\rm C}\sin^3 i_{out}$ (M$_\odot$)	1.47	0.02
$q_{\rm out}$	0.565	0.006
$rms_{\rm C}$ (km s^{-1})	8.294	
$rms_{\rm TD}$ (d)	0.0006	

Table 4: Values and standard deviations of the constrained orbital parameters for KIC 8975515.

Orbital solution A-B		
Orbital parameter	Value	Std. dev.
P (days)	1603.4	9.3
T_0 (Hel. JD)	58690.	19.
e	0.408	0.015
ω (°)	172.5	2.6
V_0 (km s^{-1})	-20.63	0.14
$a_{\rm A}\sin i$ (AU)	0.3988	0.0053
$a_{\rm B}\sin i$ (AU)	0.483	0.028
a_{TD_A} (days)	0.00230	0.00003
$K_{\rm A}$ (km s^{-1})	2.96	0.05
$K_{\rm B}$ (km s^{-1})	3.59	0.21
$M_{\rm A}\sin^3 i$ (M$_\odot$)	0.0195	0.0024
$M_{\rm B}\sin^3 i$ (M$_\odot$)	0.0161	0.0011
q	0.83	0.05
$rms_{\rm A}$ (km s^{-1})	2.597	
$rms_{\rm B}$ (km s^{-1})	0.237	
$rms_{\rm TD}$ (days)	0.00013	

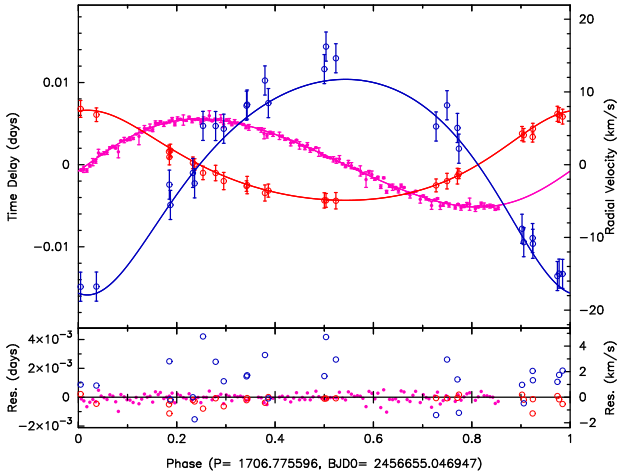

Fig. 4: Data and orbital solution for KIC 9775454. The time delays (filled pink symbols) and the radial velocities (unfilled red symbols for component A; blue symbols for component B) are overlaid with the A-B orbital solution (solid lines). The residuals are shown in the bottom panel.

well with the values proposed by Murphy et al. (2018). By treating this system as a SB2 and using the TDs, we determined for the first time a reasonable value of the mass ratio (q = 0.42 ± 0.02). In this special case where the TDs are linked with both the low- and the high-frequency regions, the more massive primary component is very probably the hybrid pulsator.

5. Discussion about the frequency spacings

In this section, we investigate the distributions of the frequency differences (aka spacings) that occur in the high-frequency regime of the Fourier transforms of each system. The aim is to identify the most frequently occurring frequency spacings for each object, and to verify whether some spacings might be related to an orbital or a rotational period. In the case of an orbital or a rotational origin of some low frequencies (e.g. due to modulations in the light curve caused by the tidal deformations or the presence of spots or surface inhomogeneities e.g. MOBSTER (Sikora et al. 2019) or caused by tidal excitation e.g. KIC 4142768 (Guo et al. 2019)), we may expect the detection of a significant number of harmonics of the corresponding main frequencies. In the case of tidal or rotational splitting of the high frequencies caused by rapid pulsations, we may expect to find regular frequency patterns whose spacing values would point at those same frequencies (e.g. KIC 6048106, Samadi Ghadim et al. 2018).

We used the detrending algorithm of Lightkurve v1.9 to detrend the *Kepler* light curves of the previously discussed systems (Barentsen & Lightkurve Collaboration 2020), and computed the periodograms with the Lomb-Scargle technique. We analysed different frequency intervals depending on where the power was located in the respective periodograms. For KIC 4480321, this was the [12.5, 24.7] d^{-1} interval; for KIC 5219533, the [6, 22.5] d^{-1} interval; for KIC 8975515, the [12.5, 17.5] d^{-1} interval and for KIC 9775454 we analysed the [5.7, 22.5] d^{-1} interval. We computed the spacings between frequency pairs, and counted the number of occurrences, adopting the limiting resolution of the *Kepler* long-cadence data (0.00068 d^{-1}) (Samadi Ghadim et al. 2018).

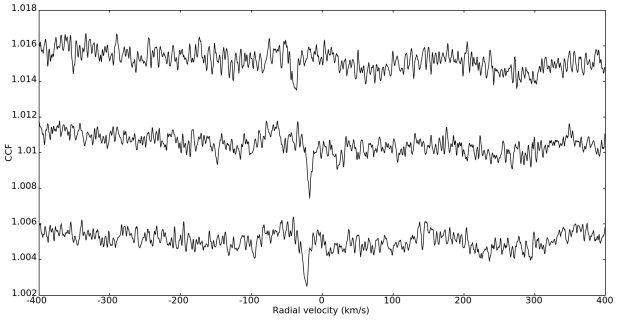

Fig. 5: Example of a cross-correlation function (CCF) of the residual spectrum of KIC 9775454 computed with a mask of spectral type K0. The shallow peak is a permanent travelling feature of the residual CCFs.

Table 5: Values and standard deviations of the constrained parameters of the orbital solution for KIC 9775454.

Orbital solution A-B		
Orbital parameter	Value	Std. dev.
P (d)	1706.8	6.4
T_0 (Hel. JD)	56655.	10.
e	0.212	0.008
ω (°)	349.6	1.9
V_0 (km s^{-1})	-22.15	0.16
$a_{\rm A}\sin i$ (AU)	0.949	0.017
$a_{\rm B}\sin i$ (AU)	2.27	0.09
$a_{\rm TD_A}$ (d)	0.00548	0.00010
$K_{\rm A}$ (km s^{-1})	6.19	0.12
$K_{\rm B}$ (km s^{-1})	14.82	0.62
$M_{\rm A}\sin^3 i$ (M$_\odot$)	1.08	0.11
$M_{\rm B}\sin^3 i$ (M$_\odot$)	0.45	0.03
q	0.42	0.02
$rms_{\rm A}$ (km s^{-1})	0.471	
$rms_{\rm B}$ (km s^{-1})	2.150	
$rms_{\rm TD}$ (d)	0.00028	

We next discuss the results of the frequency spacings derived from the *Kepler*-based periodograms for the four systems with the improved orbits. The histogram plots of the frequency spacings were produced from the counts adopting a bin size of 0.05 d^{-1} in each case. In Fig. 6, we show the distributions of the spacings for KIC 4480321, 5219533, 8975515 and KIC 9775454 in the restricted frequency range [0, 5] d^{-1}, i.e. the interval where the highest occurrences can be found. A first general observation is that the distributions of the frequency spacings in the high-frequency regime of the four systems show large differences between them. Secondly, the peak occurrence (or maximum count) of the individual spacings is generally located in the first bin. This is due to the fact that this bin contains the smallest possible spacing which corresponds to the frequency resolution of 0.00068 d^{-1}.

From the histograms of the normalized density functions presented in Fig. 6, we derive the following findings:
- KIC 4480321 presents a dense, continuous distribution of frequency spacings. The two highest occurrences, marked by the dark-grey arrows, occur at the spacings of 0.35 and 1.63 d^{-1}. The next most frequent spacing is located at 3.33 d^{-1} (marked by the dotted dark-grey arrow). The latter shows a harmonic relation with 1.63 d^{-1} (ratio of almost 2). Indeed, rotation could very well explain such a relation. The next most frequent spacings are located at 0.51, 0.74 and 2.14 d^{-1}. There is power everywhere, also in the first bin. This is due to the presence of the most frequent individual spacing which equals 0.0014 d^{-1}. However, there is no evidence of a peak occurrence near or at the orbital frequency value of 0.11 d^{-1} (the bin size could resolve this). We conclude that the orbital frequency of the close (inner) binary system does not affect the pulsation frequencies in the p-mode region. This is perfectly consistent with the conclusion that component C is the δ Scuti pulsator. As a side note, we recall that Li et al. (2020) derived 0.0070 ± 0.0007 d^{-1} for the near-core rotation rate from a modelling of the slope-period relation based on the regular period spacings in the g-mode region. Such a value stands in sharp contrast with the potential surface rotation rates derived for component C from the abovelisted most frequent spacings.
- KIC 5219533 also shows a dense distribution of spacings, though of lower density than KIC 4480321, with many (almost) equal maxima. The most frequent spacings occur at the frequencies of 0.55, 0.94 (indicated by the light blue arrows) as well as 2.32 d^{-1} (marked by the dotted light blue arrow). The orbital period of the close (inner) binary is ∼32 d, which implies that the corresponding frequency (at 0.03 d^{-1}) would be located in the first bin. Since the highest occurrence of the spacings occurs in the first bin (the most frequent individual spacing occurs at 0.0012 d^{-1}), we cannot tell from this plot whether or not this frequency is affecting the higher frequencies. However, the individual counts do not reveal the presence of a frequent spacing near the orbital frequency. The next most frequent spacings are found at 2.08 (this peak is occulted by an equal frequent spacing in green, see below), 2.98 and 3.59 d^{-1}. The frequent spacings of 0.55 and 0.94 d^{-1} could indicate the rotation period of component C. We note that Li et al. (2020) derived 0.59 ± 0.01 d^{-1} for the near-core rotation rate based on their modelling. This seems to match the smallest value of the proposed surface rotation frequencies (i.e. 0.55 d^{-1}).
- KIC 8975515 presents a continuous distribution of unequal peaks of much lower density. The two highest occurrences (except for the first bin), marked by the dark-orange arrows, occur at 2.10 and 3.76 d^{-1}, closely followed by 1.06 d^{-1}. Here again, the ratio of ∼ 2 between two of the three most frequent spacings indicates that rotation might be the relevant mechanism to explain the presence of a frequent spacing and its harmonic. However, there is also a noticeable higher occurrence of a frequent spacing located at 1.66 d^{-1}, which we know corresponds to the rotation frequency of the fast-rotating hybrid pulsating component in the system (Samadi-Ghadim et al. 2020). In addition, 1.66 d^{-1} shows the highest occurrence among the individual spacings. Li et al. (2020) derived 1.85 ± 0.01 d^{-1} for the near-core rotation rate. If this rate corresponds to the faster component, the core versus surface rotation ratio would equal 1.11 ± 0.01, as expected from the general trend found by Li et al. (2020). The frequent spacing of 1.06 d^{-1} might correspond to the more slowly-rotating δ Scuti component, although Samadi-Ghadim et al. (2020) estimated a rotation rate of 0.42 d^{-1} for this component. In this case also, the orbital frequency is not resolved.
- KIC 9775454 shows an uncommon and extremely sparse distribution in frequency spacing. The two highest occurrences (except for the first bin), marked by the green arrows, occur at the spacings of 0.13 and 2.18 d^{-1}. The latter spacing is accompanied by a few other frequent spacings located at the nearby frequencies of 2.07, 2.26 and 2.35 d^{-1}. It is tempting

to interpret one of these frequent spacings as the rotational frequency of the pulsating component (comp A) (with obvious variability in the case of 2 d^{-1}). The orbital frequency is beyond the frequency resolution here as well.

In summary, we found no indication for the presence of any tidal frequency splitting due to the close (inner) orbits in the high-frequency regime of the hybrid stars which belong to triple systems. In the case of the long-period orbits (all systems), we cannot tell as it is impossible to resolve the frequency multiplets based on the *Kepler* data only. On the other hand, there is evidence for the presence of rotational splitting in the systems KIC 4480321 and KIC 8975515. Such an explanation may also be relevant in the two other systems that we studied closely, namely KIC 5219533 and KIC 9775454.

6. Discussion and conclusions

In the previous sections, we improved the orbital solutions for four spectroscopic systems from our sample of 49 A/F-type *Kepler* hybrid stars. We improved the orbital solutions for the following spectroscopic systems: KIC 4480321, 5219533, 8975515 and KIC 9775454 by considering the TDs as well as the RVs and performing a simultaneous modelling of both data types. This method allowed us to refine the parameters of all the long-period systems, in particular the outer orbits of the triple systems KIC 4480321 and KIC 5219533. We derived full-fledged SB2 orbital solutions for the long-period binary systems KIC 8975515 and KIC 9775454 and obtained reliable mass ratios for the first time. Furthermore, the applied methodology enabled us to identify the component with the faster δ Sct-type pulsations, since the TDs are generally linked with the higher frequencies.

For KIC 4480321, we concluded that the faster rotating and more massive outer component (comp C) exhibits the short-period δ Scuti pulsations. Component C was shown to have a minimum mass of 1.60 ± 0.05 $M_\odot$, which can be used as a constraint for asteroseismic modelling. For KIC 5219533, we significantly improved the accuracy of the orbital solutions described by Catanzaro et al. (2019b). We also showed that both orbits are very probably coplanar and that the δ Scuti pulsator is the faster spinning and more massive outer component (comp C). For KIC 8975515, we derived an accurate mass ratio (q = 0.83 ± 0.05) and established that the faster rotating component (comp A) exhibits δ Scuti-type pulsations (this concerns the hybrid pulsator). Furthermore, the binary is probably viewed under a low inclination angle (≈ 12°). The latter is also useful information in an asteroseismic context. For KIC 9775454, we determined a precise mass ratio for the first time (q = 0.42 ± 0.02). We concluded that the more massive component of the system (comp A) is the hybrid pulsating star.

From our study of the normalized distributions of the frequency spacings which led to the identification of the most frequent spacings in the high-frequency regime of the Fourier transforms of each system, we conclude that there is no firm evidence for tidal frequency splitting among the frequent spacings of the systems with close companions. On the other hand, we clearly detected indications of rotational splitting for the systems KIC 4480321 (with a possible rotation rate of 1.63 d^{-1}), and KIC 8975515 (with rotation rates of 1.66 d^{-1} and possibly 1.06 d^{-1}). We furthermore suggest possible rotational splitting for KIC 5219533 (with a rotation rate of 0.55 d^{-1}) and perhaps for KIC 9775454.

Acknowledgements

The authors wish to thank the *Kepler* team for providing the high-quality data collected with the *Kepler* satellite mission. They also thank the HERMES Consortium for enabling the collection and production of the high-resolution ground-based spectra. ÁS and ZsB acknowledge financial support of the Lendület Program LP2018-7/2019 of the Hungarian Academy of Sciences. MS acknowledges the OV PPP PostdocMUNI grant with nr. CZ.02.2.69/0.0/0.0/16_027/0008360. ZsB acknowledges the support provided from the National Research, Development and Innovation Fund of Hungary, financed under the PD_{17} funding scheme (project PD-123910) and the support by the János Bolyai Research Scholarship of the Hungarian Academy of Sciences. HL acknowledges support from the grant DFG LE1102/3-1. ASG acknowledges financial support received from the ALMA-CONICYT grant with nr. 31170029. We are furthermore grateful for financial support received from the Belgo-Indian Network for Astronomy & Astrophysics (networking projects BINA-1&2).

References

Balona, L. A., Daszyńska-Daszkiewicz, J., & Pamyatnykh, A. A. 2015, MNRAS, 452, 3073
Barentsen, G. & Lightkurve Collaboration. 2020, in American Astronomical Society Meeting Abstracts, American Astronomical Society Meeting Abstracts, 409.04
Castelli, F. & Kurucz, R. L. 2003, in IAU Symposium, Vol. 210, Modelling of Stellar Atmospheres, ed. N. Piskunov, W. W. Weiss, & D. F. Gray, A20
Catanzaro, G., Gangi, M., Giarrusso, M., Munari, M., & Leone, F. 2019a, MNRAS, 488, 480
Catanzaro, G., Gangi, M., Giarrusso, M., Munari, M., & Leone, F. 2019b, MNRAS, 487, 919
Fauvaud, S., Rodríguez, E., Zhou, A. Y., et al. 2006, A&A, 451, 999
Fauvaud, S., Sareyan, J. P., Ribas, I., et al. 2010, A&A, 515, A39
Gaia Collaboration. 2018, VizieR Online Data Catalog, I/345
Grigahcène, A., Antoci, V., Balona, L., et al. 2010, ApJ, 713, L192
Guo, Z., Fuller, J., Shporer, A., et al. 2019, ApJ, 885, 46
Hubeny, I. & Lanz, T. 1995, ApJ, 439, 875
Irwin, J. B. 1952, Publications of the Goethe Link Observatory, 8, 77
Lampens, P., Frémat, Y., Vermeylen, L., et al. 2018, A&A, 610, A17
Li, G., Bedding, T. R., Murphy, S. J., et al. 2019, MNRAS, 482, 1757
Li, G., Van Reeth, T., Bedding, T. R., et al. 2020, MNRAS, 491, 3586
Murphy, S. J., Bedding, T. R., Shibahashi, H., Kurtz, D. W., & Kjeldsen, H. 2014, MNRAS, 441, 2515
Murphy, S. J., Moe, M., Kurtz, D. W., et al. 2018, MNRAS, 474, 4322
Murphy, S. J. & Shibahashi, H. 2015, MNRAS, 450, 4475
Murphy, S. J., Shibahashi, H., & Bedding, T. R. 2016, MNRAS, 461, 4215
Nielsen, M. B., Gizon, L., Schunker, H., & Karoff, C. 2013, A&A, 557, L10
Pribulla, T., Chochol, D., Tremko, J., & Kreiner, J. M. 2005, in Astronomical Society of the Pacific Conference Series, Vol. 335, The Light-Time Effect in Astrophysics: Causes and cures of the O-C diagram, ed. C. Sterken, 103
Raskin, G., van Winckel, H., Hensberge, H., et al. 2011, A&A, 526, A69
Renson, P. & Manfroid, J. 2009, A&A, 498, 961
Samadi Ghadim, A., Lampens, P., & Jassur, D. M. 2018, Acta Astron., 68, 425
Samadi-Ghadim, A., Lampens, P., Jassur, D. M., & Jofré, P. 2020, A&A, 638, A57
Shibahashi, H. & Kurtz, D. W. 2012, MNRAS, 422, 738
Sikora, J., David-Uraz, A., Chowdhury, S., et al. 2019, MNRAS, 487, 4695
Uytterhoeven, K., Moya, A., Grigahcène, A., et al. 2011, A&A, 534, A125

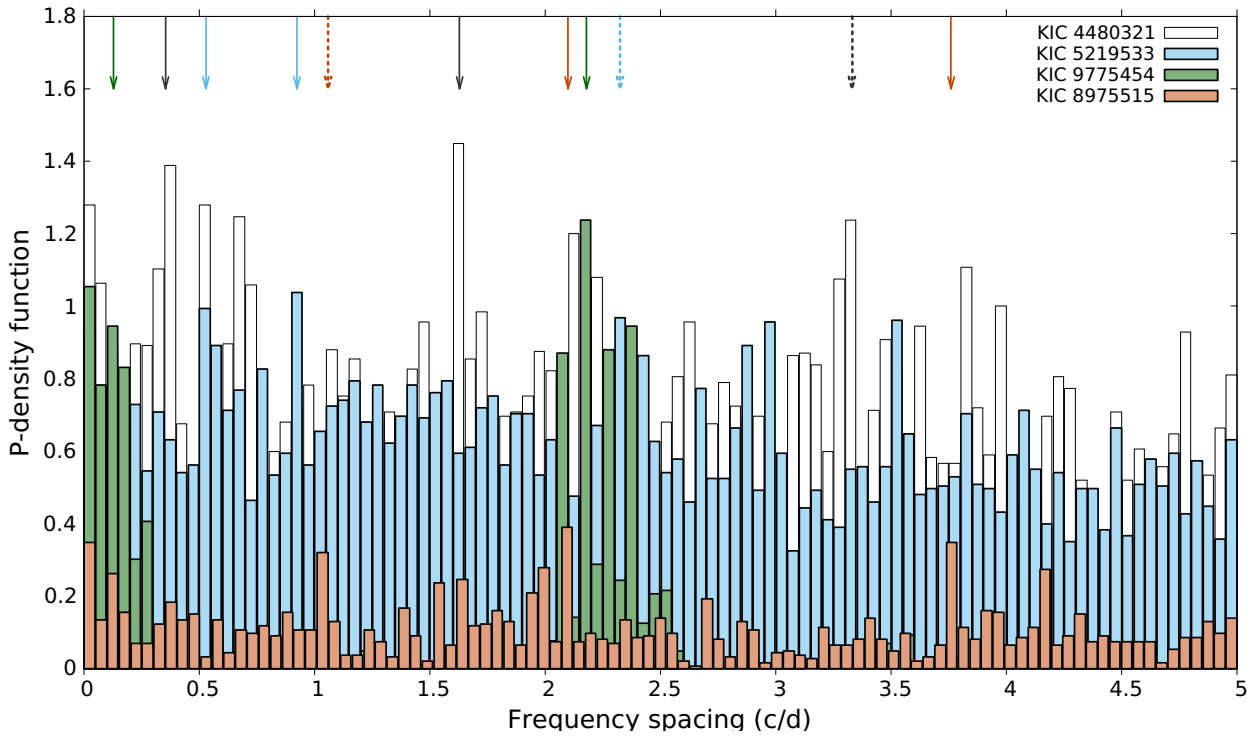

Fig. 6: Distributions of the frequency spacings derived from the *Kepler*-based periodograms for the four discussed systems.